

## Supplementary data

### Experimental Section: Characterization

The additives temperature stability was analyzed by Thermogravimetric Analysis (TGA) with a TG Discovery from TA Instruments. The analyses were performed from ambient to 450 °C under an argon flow of 25 mL/min and at a heating rate of 2 °C/min. Hermetic aluminium pans with a pin hole, sealed inside the glove box, were used to prevent any oxidation.

The XRD structural characterization of the samples was carried out with a Bruker D8 Advance A25-ray diffractometer using Cu-K $\alpha$  radiation. The diffraction patterns were analysed by the Rietveld method using the Topas software allowing determination of the phase composition and crystallites mean size. X-ray sample holders were filled inside the glove box and covered with a kapton foil to minimize oxidation during X-ray measurements.

The sample morphology was characterized by Scanning Electron Microscopy (SEM) with a Philips 5800 apparatus. Transmission Electron Microscopy (TEM) was also performed with a JEOL 2010 LaB6 apparatus. Ethanol dispersion of the powders on carbon grids was used to prepare the samples. The mean size and size distribution of the MgH<sub>2</sub> particles was determined with the SEM images by counting the particles using ImageJ software. Also, an Energy-dispersive X-ray (EDX) analysis was carried out in parallel with TEM measurements in order to determine the presence of different elements in the samples (e.g. Ru, O, Mg...).

X-ray photoelectron spectroscopy (XPS) was carried out with a KRATOS AXIS Ultra DLD spectrometer equipped with a magnetic immersion lens, a hemispherical analyzer and a delay line detector. The base pressure in the analysis chamber was 5 10<sup>-10</sup> mbar. All the data were acquired using a monochromated Al K $\alpha$  X-ray source (1486.6 eV, 150 W) at a normal angle with respect to the surface. The analyzer was operated at 160 eV pass energy for acquisition of survey scans and at 20 eV pass energy for acquisition of high-resolution spectra of Ru 3d, P 2p, C 1s and O 1s core levels. Charge neutralization was used to compensate charging of the samples and the area analyzed was 700  $\mu$ m  $\times$  300  $\mu$ m.

The <sup>13</sup>C and <sup>31</sup>P solid NMR experiments were performed on a Bruker Avance III 500WB spectrometer at 125.7 and 202.4 MHz, respectively or on a Bruker Avance III 400 spectrometer at 100.48 and 161.76 MHz, respectively, equipped with a 3.2 or 4 mm probe. The chemical shifts of <sup>31</sup>P nuclei are given relative to H<sub>3</sub>PO<sub>4</sub> at 0 ppm.

### Experimental Section: Storage properties

The Kissinger equation (S1) allows the determination of the activation energy for a decomposition reaction regardless to the reaction order. The linearization of the Kissinger equation in logarithmic form is reported as follows:

$$\ln\left(\frac{\beta}{T^2}\right) = -\frac{E_a}{T} + \ln\left(\frac{RC_0}{T^2E_a}\right) \quad (S1)$$

with R the gas constant,  $\beta$  the heating rate,  $C_0$  the reaction order, and T the temperature of the DSC peak. The activation energy values are obtained from the slope of the straight lines interpolating the data obtained by plotting  $\ln(\beta/T^2)$  versus  $1000/T$  for each sample.

The absorption and desorption enthalpies and entropies were calculated using the Van't Hoff equation (S2):

$$\ln\left(\frac{P_{eq}}{P_0}\right) = \frac{\Delta H_0}{RT} - \frac{\Delta S_0}{R} \quad (S2)$$

with R the gas constant,  $P_{eq}$  the pressure at the equilibrium plateau,  $P_0$  the atmospheric pressure, and T the temperature of the isotherm. The enthalpies and entropies values are obtained from the slope of the straight lines interpolating the data obtained by plotting  $\ln(P_{eq}/P_0)$  vs  $1/T$  for each sample.

## Results Section:

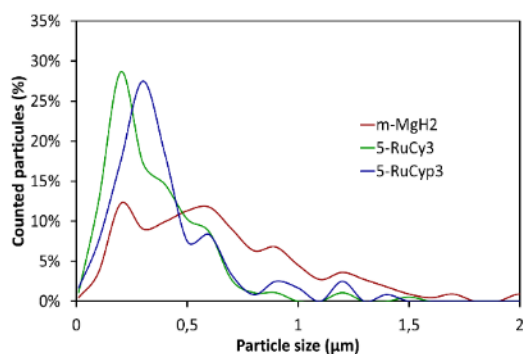


Fig. S1 Size distribution of  $\text{MgH}_2$  particles within the samples, measured by SEM analyses

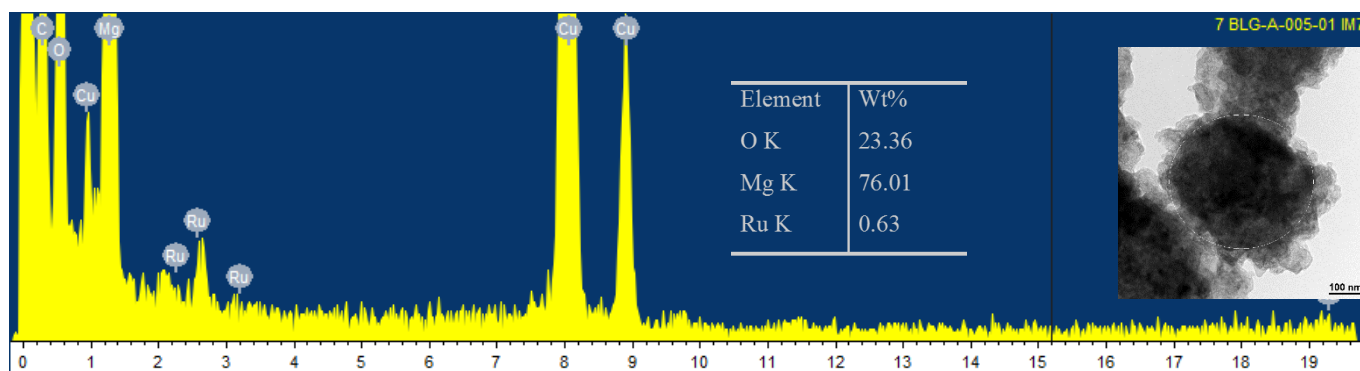


Fig. S2 EDX spectra of 5-RuCy3 and corresponding TEM image

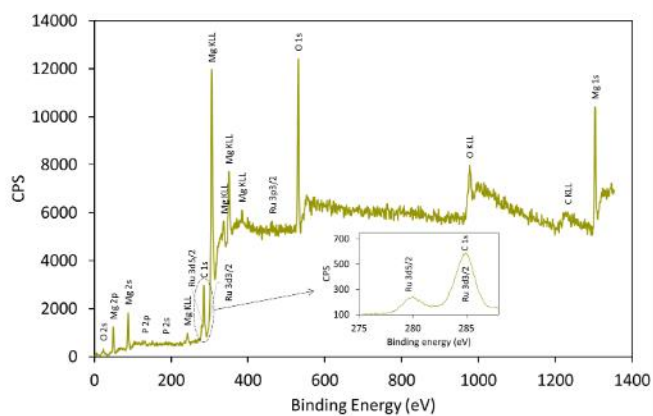


Fig. S3 XPS analysis of 20-RuCy3 sample just after milling

The high resolution Ru 3d XPS spectrum given in Fig. S3 shows a band at 279.6 eV which can be assigned to  $\text{Ru}^0$   $3d_{5/2}$  by comparing with the value of ruthenium metal at 279.7 eV (D. J. Morgan, *Surf. Interface Anal.*, 2015, 47, 1072–1079.). The  $\text{Ru}3d_{3/2}$  peak overlaps with the C1s peak in the range of 282 - 288 eV and cannot, with certainty, be assigned to  $\text{Ru}^0$  or to ruthenium in other oxidation states.

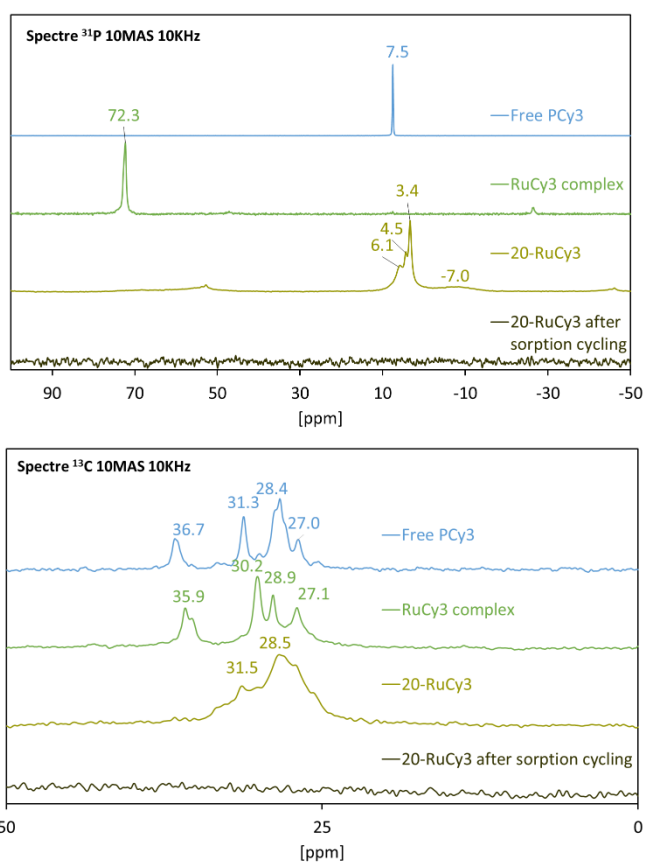


Fig. S4  $^{13}\text{C}$  and  $^{31}\text{P}$  NMR spectra of free PCy3, RuCy3 complex and 20-RuCy3 sample, comparison before and after sorption cycling

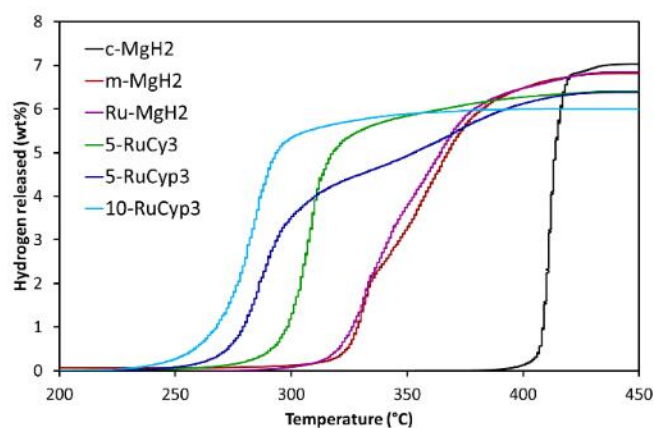


Fig. S5 Thermally programmed  $H_2$  desorption capacities curves of studied  $MgH_2$ -based powders

The curves in Fig. S5 are obtained by the integration of the TPD peaks (Fig. 5) using a calibration factor of  $5.29 \times 10^{-8}$  mmol  $H_2$ /mV.s obtained with a reference and considering the contribution of the complex decomposition negligible. Indeed, although the decomposition of the complexes is observed to occur at similar temperatures as  $MgH_2$  (see Figs. 2 and 5), Fig. S6 shows that the TCD signal of 5-RuCy3 is almost 70 times more intense than that obtained for RuCy3 complex alone.

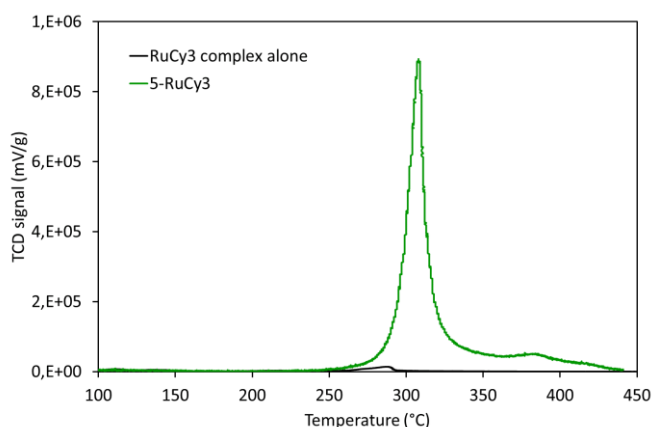


Fig. S6 Comparison of the TCD signal for 5-RuCy3 sample with RuCy3 complex alone, TPD analyses,  $2^\circ C/min$

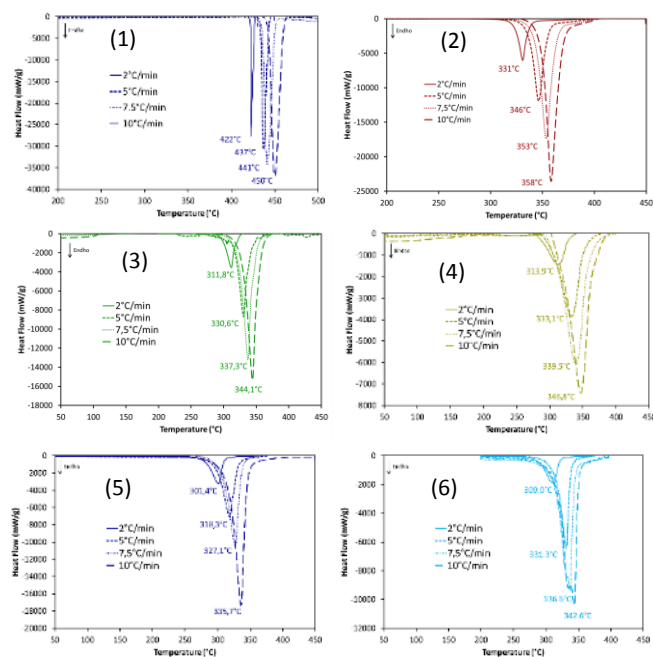


Fig. S7 DSC curves of (1) c- $MgH_2$ ; (2) m- $MgH_2$ ; (3) 5-RuCy3; (4) 20-RuCy3; (5) 5-RuCyp3 and (6) 10-RuCyp3 at different heating rates

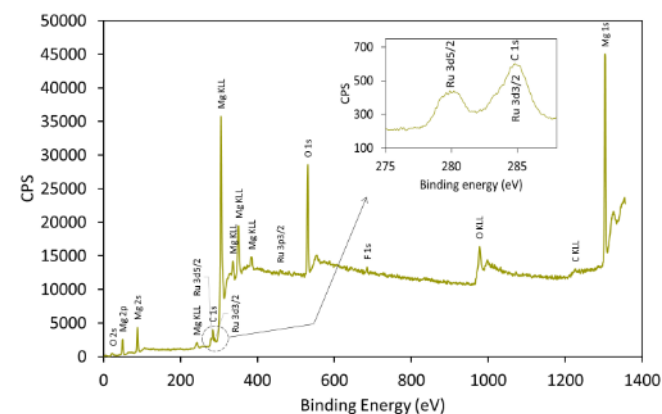


Fig. S8 XPS analysis of 20-RuCy3 sample after sorption cycling

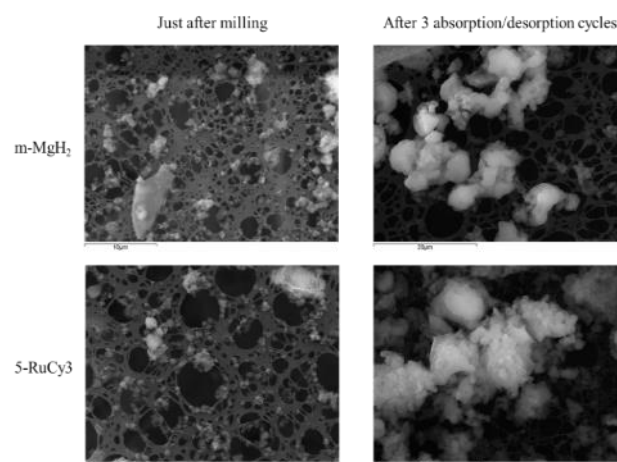


Fig. S9 SEM images before and after 3 absorption/desorption cycles at  $300^\circ C$

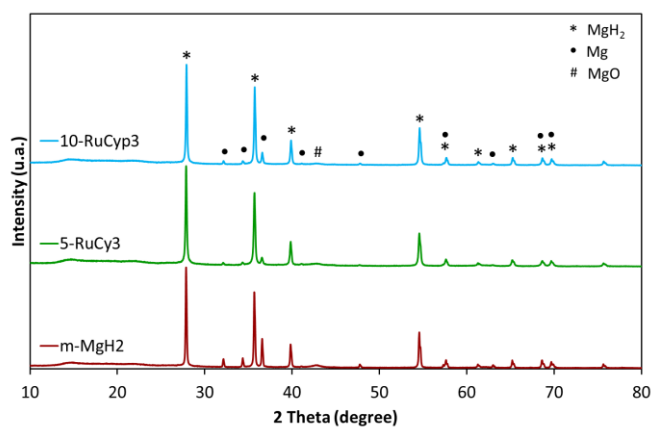


Fig. S10 X-ray diffraction patterns of the samples after sorption cycling

Table S1 Average crystal sizes of the samples after sorption cycling

| Samples            | Mean crystal size after milling (nm) | Mean crystal size after sorption cycling (nm) |
|--------------------|--------------------------------------|---|
| 10-RuCyp3          | 12 ± 7                               | 84 ± 12                                       |
| 5-RuCy3            | 14 ± 6                               | 64 ± 12                                       |
| m-MgH <sub>2</sub> | 34 ± 13                              | 85 ± 6  |

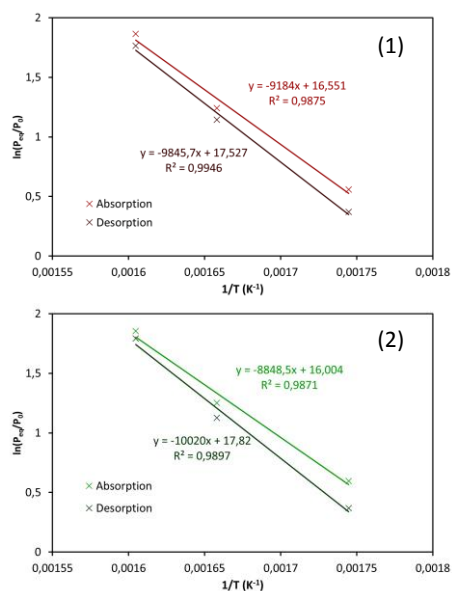


Fig. S11 Van't Hoff plots of (1) m-MgH<sub>2</sub> and (2) 5-RuCy3